Importance of the number emission factor of combustion-generated aerosols from nano-enabled products

Tobias Hammer
Institute of Environmental Engineering, ETH Zürich, 8093 Zürich/ Switzerland, Laboratory of Advanced Analytical Technologies, Empa, 8600 Dübendorf/ Switzerland

Nathan Bossa
Leitat Technological Center, 08225 Terrassa (Barcelona)/Spain

Michael Persson
Nouryon PPC AB, 445 80 Bohus/ Sweden

Adrian Wichser
Laboratory of Advanced Analytical Technologies, Empa, 8600 Dübendorf/ Switzerland

Ken Lehner
Laboratory of Advanced Analytical Technologies, Empa, 8600 Dübendorf/ Switzerland

Emmanuel Ruggiero
BASF SE, 67056 Ludwigshafen am Rhein/ Germany

Ana Sofia Fonseca
National Research Centre for the Working Environment (NRCWE), Lerso Parkallé 105, DK-2100 Copenhagen/ Den-mark

Milijana Jovic
Laboratory of Advanced Fibers, Empa, 9014 Sankt Gallen/ Switzerland

Sabyasachi Gaan
Laboratory of Advanced Fibers, Empa, 9014 Sankt Gallen/ Switzerland

Wendel Wohlleben
BASF SE, 67056 Ludwigshafen am Rhein/ Germany

Jing Wang (jing.wang@ifu.baug.ethz.ch)
Institute of Environmental Engineering, ETH Zürich, 8093 Zürich/ Switzerland, Laboratory of Advanced Analytical Technologies, Empa, 8600 Dübendorf/ Switzerland

---

Research Article

Keywords: nanomaterial, release of nanomaterials, combustion, categorization of nano-enabled products

Posted Date: December 17th, 2020

DOI: https://doi.org/10.21203/rs.3.rs-128400/v1

Importance of the number emission factor of combustion-generated aerosols from nano-enabled products

Tobias Hammer[1,2], Nathan Bossa[3], Michael Persson[4], Adrian Wichser[2], Ken Lehner[2], Emmanuel Ruggiero[5], Ana Sofia Fonseca[6], Milijana Jovic[7], Sabyasachi Gaan[7], Wendel Wohlleben[5], Jing Wang[1,2*]

[1]Institute of Environmental Engineering, ETH Zürich, 8093 Zürich/ Switzerland,

[2]Laboratory of Advanced Analytical Technologies, Empa, 8600 Dübendorf/ Switzerland,

[3]Leitat Technological Center, 08225 Terrassa (Barcelona)/Spain,

[4]Nouryon PPC AB, 445 80 Bohus/ Sweden,

[5]BASF SE, 67056 Ludwigshafen am Rhein/ Germany,

[6]National Research Centre for the Working Environment (NRCWE), Lerso Parkallé 105, DK-2100 Copenhagen/ Denmark,

[7]7Laboratory of Advanced Fibers, Empa, 9014 Sankt Gallen/ Switzerland

* Jing Wang: jing.wang@ifu.baug.ethz.ch

Abstract

Accidental or open waste burning and incineration of nano-enabled products (NEPs) might lead to the release of incidental nanomaterials (NMs) into the environment resulting in harmful effects on humans.

We have investigated combustion-generated NM release during accidental burning for several real-life NEPs such as paints with silica (SiO_2) and spruce wood panels containing SiO_2 and Fe_2O_3 NMs, paper with SiO_2 and Fe_2O_3 NMs and polymeric composites with CuPhthtalocyanine NMs in poly lactic acid (PLA), polyamide 6 (PA6) and thermoplastic pol-urethane (TPU) matrices.

Chemical compositions, aerosols number emission factors (n_{efs}) and concentrations of the signature elements of the NMs of the combustion-generated aerosols were investigated. In addition, the residual ash was analyzed. The outcomes of this study shed light on how NM and matrix types influenced the properties of the released aerosols. Based on our results it was established that the combustion-generated aerosols were composed of transformed NMs with modified physical-chemical characteristics compared to the pristine NMs. In addition to the transformed NMs, there were also particles due to incomplete combustion of the matrix.

Types of the pristine NMs and matrices affected the characteristics of the released aerosols. Since the hazard of the aerosols is related to the inhaled aerosol number concentration, the n_{ef} is an important parameter. Our results showed that the n_{efs} in the size range of 5.6 to 560 nm depended strongly on the type of combusted NEP, which indicated that the NEPs could be categorized according to their potential to release aerosols in this size range when they were burnt. The generated release data facilitate the assessment of human and environmental exposure and the associated risk assessment of combustion-generated aerosols from NEPs.

Graphical abstract

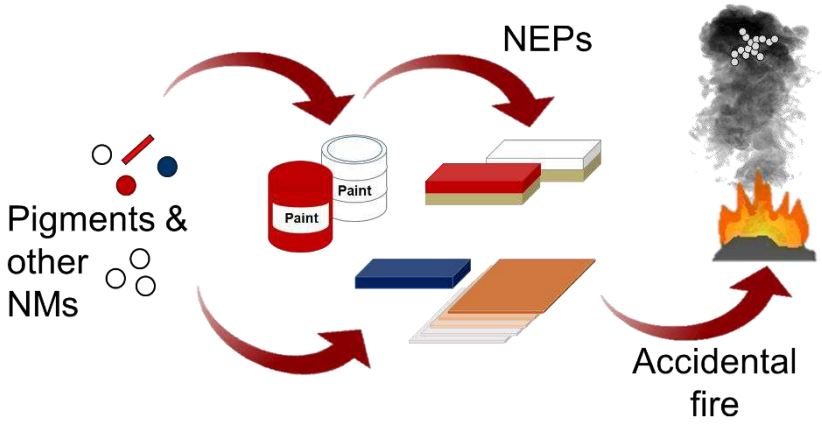

Keywords

nanomaterial, release of nanomaterials, combustion, categorization of nano-enabled products

1. Introduction

To take advantage of the extraordinary physical-chemical properties of nanomaterials (NMs), the amount of NMs used in consumer and industrial applications is continuously increasing (Breuer and Sundararaj 2004, Nowack and Bucheli 2007, Potts et al. 2011, Limited 2011, Le et al. 2014, Singh et al. 2016, Gonçalves et al. 2018). Graphene nanoplatelets or carbon nanotubes show high electrical and thermal conductivity (Potts et al. 2011, Wang et al. 2017). NM pigments such as CuPhthalocyanine or Fe_2O_3 have extremely intense color due to their excellent light-scattering properties (Kotnarowska et al. 2014) and SiO_2 nanoparticles have high mechanical stability (Mahrholz et al. 2009, Sow et al. 2011). To profit from these properties, NMs are applied in so-called nano-enabled products (NEPs) such as construction materials, paints, paper, cosmetics, sports products or in airplanes or automobiles (Kittelson et al. 2004, Nowack and Bucheli 2007, Kuhlbusch et al. 2010, Brar et al. 2010, Sow et al. 2011, Bello et al. 2013, Wang et al. 2017, Part et al. 2018, Surendhiran et al. 2020). According to Madkour 2019, the global nanotechnology revenue is tremendously growing since about 1995.

Apart from the benefits, NMs or NEPs might also have adverse effects. During the entire life cycle of a NEP, NMs can be released and human beings or the environment can be exposed and harmfully affected (Froggett et al. 2014, Seipenbusch et al. 2014, Nowack and Bucheli 2007, Nowack et al. 2012, Roes et al. 2012). During the use phase, NM release can occur e.g. by material aging induced by weathering, or by mechanical treatment (abrasion, drilling, sawing, etc.). At the end of their life, NMs or NEPs are either directly disposed in a landfill or thermally decomposed in open waste burning or in waste incineration plants (Keller and Lazareva 2014). Vejerano et al. (2014) found that 8600 tons of NMs were expected to be incinerated globally per year with increasing tendency. High temperatures and fragmentation and oxidation processes during the combustion lead to thermal decomposition of the NEPs and the release of incidental, process-generated nanoparticles in the form of fly ash into the air (Chivas-Joly et al. 2014, Wang et al. 2017, Singh et al. 2017, Singh et al. 2019, Hansen et al. 2015).

One of the most critical exposure routes for humans to such aerosols is the exposure pathway of inhalation, since the inhaled particles might deposit in the alveoli and the trachea bronchus of the respiratory system or can even penetrate into the blood (Rothen-Rutishauser et al. 2006). Once in the bloodstream the NMs are circulated in the whole body and could be transferred to vital organs such as brain or heart, where an agglomeration of the NMs can lead to severe diseases such as apoplexy or heart attacks (Rothen-Rutishauser et al. 2006, Pope, et al. 1995, Schulz et al. 2005). Toxicity and biological effects of the inhaled aerosols depend strongly on their concentration, as well as size, shape and chemical composition.

Since inhalation is the most probable exposure pathway to combustion-generated NMs (Basinas et al. 2019), and the combustion-generated aerosol NMs might induce different adverse effects than the pristine NMs, aerosol concentrations and their physical-chemical properties need to be assessed (Roes et al. 2012). It is simplistic to take only the type of NM (organic, inorganic, chemical composition) into account for the risk assessment. Also other parameters such as the product matrix or the combustion parameters should be considered. The hazard of the aerosols

99 is directly related to the inhaled aerosol dose, which depends on the inhaled aerosol concentra-
100 tion (Hammer et al. 2020). The potential to release aerosols during the combustion could de-
101 pend on the type of NEP burnt. Classification of the NEPs by similarity and read-across would
102 save time and allow an effective risk assessment of the released aerosol NMs. Studies on aerosol
103 release during accidental burning of real NEPs are still scarce and new and more data are needed
104 to classify the NEPs.

105 Several studies (Wang et al. 2017, Chivas-Joly et al. 2019, Oischinger et al. 2019, Walser et al.
106 2012, Mitrano et al. 2015, Hansen et al. 2015) reported that the combustion-generated NMs
107 show strongly transformed physical-chemical characteristics compared to the pristine NMs.
108 Following the source-to-adverse-outcome pathway (SAOP) approach described by Oomen et
109 al. (2015) and Landsiedel (2016), every modification of the physical-chemical properties of a
110 NM needs to be taken into consideration for a risk assessment, since the physical-chemical
111 properties of the generated NM define its final toxicity and its biological impact.

112 Combustion-induced NM release was studied previously for the incineration of municipal waste
113 with TiO_2, ZnO, Ag and CeO_2 NMs (Mueller et al. 2013, Buha et al. 2014). Mueller et al. (2013)
114 showed that the major fraction of the NMs (TiO_2, ZnO and Ag) went to the residual bottom ash
115 and only a small fraction was released as fly ash. Buha et al. (2014) concluded that the opera-
116 tional conditions for the incineration (temperature, pressure, etc.) and the type of incinerated
117 material (waste, NM) determined the chemical composition of the residual ash and the gener-
118 ated aerosol.

119 Singh et al. (2019) found that the operation conditions of the combustion affected the release
120 of NMs. At a temperature of 500 °C, inorganic NMs such as CuO, Fe_2O_3, SiO_2 stayed in the
121 residual ash, whereas organic NMs e.g. DPP (diketopyrrolopyrrole) Red were decomposed and
122 transformed into soot and CO_2. At a temperature of 850 °C in incineration plants, the inorganic
123 nanofillers remained mainly in the residual ash and only small concentrations of Cu and Fe

signature elements of CuO and Fe_2O_3 were detected in the aerosols. Schlagenhauf et al. (2015), who incinerated epoxy composites with multi-walled carbon nanotubes (CNTs), showed that the oxygen content of the combustion air affected the final appearance, the total particle concentration and the chemical composition of the fly ash. Massari et al. (2014) found that TiO_2 nanoparticles from solid paints were strongly physical-chemically modified and sintered with other ash residues and remained in the residual ash after the incineration using an incineration temperature of 950°C.

Release of so-called LCPM (life cycle particulate matter) that represents fly ash particles and residual ash has been investigated under lab-scale conditions for combusted polymer-based NEPs and nano-enabled coatings (NECs) with CNTs, CuO, Fe_2O_3, SiO_2 NMs (Sotiriou et al. 2015, Sotiriou et al. 2016, Singh et al.2016, Singh et al. 2017, Singh et al. 2019). According to Singh et al. (2019), the higher the NM loadings in a NEP, the higher were the concentrations of the signature elements of the pristine NMs found in the fly ash. Moreover, the host matrix seemed to strongly affect the chemical composition of the LCPM (Sotiriou et al. 2016, Singh et al.2016, Singh et al. 2017, Singh et al. 2019).

In this work we have investigated combustion-induced NM release during accidental / outdoor burning for several real-life NEPs such as applied paints containing SiO_2 or Fe_2O_3 NMs on spruce wood panels, paper with SiO_2 and Fe_2O_3 NMs and polymeric composites with CuPhthtalocyanine NMs in poly lactic acid (PLA), polyamide 6 (PA6) and thermoplastic polyurethane (TPU) matrices. The combustion conditions included the oxygen concentration of ambient air (20.95 %) and a temperature of 570°C. These conditions were intentionally different from the legally required conditions of waste incineration.

We compared the physical-chemical characteristics of the released particles and pristine NMs, to determine whether the pristine NMs were released in the fly ash. Moreover, the effects of types of matrices and NMs on the amount and the shape of the released aerosol were evaluated.

By comparing aerosol number emission factors (n_{efs}), which were defined as the average emitted aerosol number per gram burnt NEP, we were able to assess the potential of the NEPs to release aerosols during combustion. Physical-chemical data and n_{efs} facilitate the evaluation of the NM environmental release and workers' or consumers' exposure potential during the combustion of such materials and allow in combination with literature data a more comprehensive assessment of environmental health and safety.

2. Materials and methods

2.1 Pristine nanomaterials and nano-enabled products

Three different types of real-world NEPs were subjected to combustion: polymeric composites, wood panels with applied paints and paper. The NEPs contained NMs with high production volumes such as Fe_2O_3, SiO_2 and CuPhthalocyanine (Ministère de l'Environnement 2015, Ruggiero et al. 2019, Wigger et al. 2018). Two different crystalline forms of CuPhthalocyanine NMs (α and β) were embedded in polymeric composites whereas different types of Fe_2O_3 and SiO_2 NMs were used in paints and papers. More details may be referred to the supplementary Table S1.

2.2 Setup of the combustion experiment and online particle detection

We employed a Cone Calorimeter (Fire Testing Technology, FTT, GB) with a heat flux of 25 kW/m^2 resulting in a temperature of about 570°C for the combustion and followed ISO 5660 ASTM E 1354 to simulate the burning of the NEP. The oxygen concentration of the air was 20.95 %. The fuming samples were ignited through an electric spark, generated by an ignitor, at a distance of 0.3 cm without direct contact to the samples. A standardized sample surface area of 10 cm × 10 cm was used. Polymeric composites samples had a thickness of 0.3 cm and wood panels with applied paint had a thickness of 1.5 cm. Stacks of five paper sheets with a total thickness of 0.1 cm corresponded to one paper sample. The emitted aerosols were sampled through a circular inlet with a diameter of 5 mm, diluted with filtered ambient air and transferred to the analytical instruments through a tubing system made of stainless steel.

Emitted aerosol size distributions (ASDs) in the size range of 5.6 nm to 560 nm were analyzed with 1 Hz frequency by using a fast mobility particle sizer (FMPS 3091, TSI). The ASDs in the size range of 542 nm to 20 µm were scanned using an aerodynamic particle sizer (APS 3321, TSI) with scanning periods of 20 seconds. Continuously, ASDs were detected until the burning samples extinguished. The combustion experiments were repeated 3 times and the total aerosol concentrations of the FMPS and APS measurements were averaged per second. Prior to the experiment, when there was no combustion, background concentrations were measured for similar durations as for the respective samples, corresponding to about 150 s for paper samples, to 8 min for polymeric composite samples and to 17 min for wooden panels with applied paints. The background concentrations were subtracted from the aerosol concentrations from the experimental measurements with the samples.

The emitted fly ash was collected on Nuclepore filters with a pore size of 0.2 µm (Whatman, UK) for offline analyses. Scanning electron microscope (SEM) was used to investigate the shape and the size of the released fly ash particles and electron dispersive X-ray-SEM (EDX-SEM) and inductively coupled plasma-mass spectroscopy (ICP-MS) were used to assess the chemical composition. The residual ash was also collected and investigated via EDX-SEM. For more details on the morphology evaluation, may be referred to the supplementary information. Fig. 1 shows the experimental setup for the combustion tests.

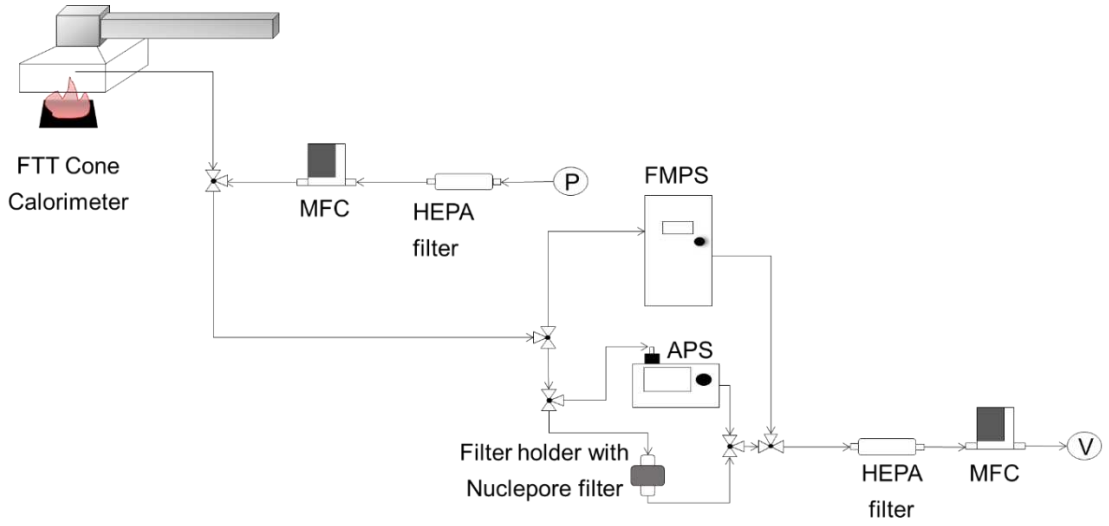

Fig. 1. Setup used for combustion experiments, aerosol measurement and fly ash collection with Cone Calorimeter (FTT), mass flow controllers (MFCs), HEPA filters, fast mobility particle sizer (FMPS), aerodynamic particle sizer (APS), filter holder with Nuclepore filter (Whatman, UK) with a pore size of 0.2 µm, pump (P) and vacuum pump (V).

2.3 Determination of the aerosol number emission factors (n_{efs})

The aerosol number emission factors (n_{efs}) correspond to the potential of a NEP to release aerosols during the combustion. The n_{efs} were calculated for the FMPS size range of 5.6 nm to 560 nm and the APS size range of 542 nm to 20 µm by using equation (1). Potential particle losses in the tubes of the combustion setup was assumed to be similar for the different samples and neglected in the calculation.

(1) $$\boldsymbol{n_{efs} = \frac{ct}{ms} \times vi \times t \times df \times cf}$$

with *ct* averaged total concentration in the instrument range (FMPS or APS) in #/cm^3, *ms* burnt sample mass in g, *vi* volume flowrate to the instrument in cm^3/s (FMPS: 133.3; APS: 16.6), *t* duration of incineration in s, *df* dilution factor (FMPS: 1.75; APS: 14) equal to the total flowrate through the system divided by the flowrate of the instrument, *cf* correction factor equal to the volume flowrate to the exhaust fan of the Cone Calorimeter divided by the flowrate of the instrument to compensate the divergence of the flow rates (FMPS: 180; APS: 960).

2.4 Qualitative determination of the chemical composition of the fly ash and the residual ash

The chemical composition of the fly ash was scanned at several locations using EDX-SEM (environmental scanning electron microscopy ESEM, Thermo Fisher Quanta 650) with a 10 kV

acceleration voltage. EDX analyses of the residual ash were done using SEM Phenom ProX (Phenom) with an acceleration voltage of 10 kV. The measured values were averaged over three spots on the SEM images.

2.5 Quantitative determination of the chemical composition of the fly ash by ICP-MS

ICP-MS NexION 2000 (Perkin Elmer) was employed for quantitative analyses of the chemical composition of the fly ash. Fly ash particles on circular filter sections with a diameter of 8 mm were digested using the microwave MLS 1200 mega (MLS) and by applying an inverse king's water (mixture of 3 ml of concentrated nitric acid 67 % (VWR) and 1 ml of concentrated hydrochloric acid (VWR)). The digested samples did not show any precipitation. As a blank reference, the Nuclepore filter was analyzed in a separate measurement. The detected trace elements were subtracted from the elemental composition of the samples, giving rise to the release concentration of the signature elements of the NMs such as Cu, Fe and Si. The lowest limits of detection (LODs) were calculated using the threefold standard deviation of the detected values of the blank solutions. LODs: Cu: 0.276 µg/filter, Si: 0.078 µg/filter, Fe: 0.014 µg/filter, equaling to Cu: 5.80 ng/g fly ash from polymers, to Si: 1.12 ng/g fly ash from white paint with silica, to Si: 21.5 ng/g fly ash from paper with silica, to Fe: 0.21 ng/ fly ash from red paint and to Fe: 3.86 ng/ fly ash from paper with iron oxide.

3 Experimental results

3.1 Aerosol number emission factors

Fig. 2 shows the n_{efs} of combustion-generated aerosols from paper, polymeric composites, and applied paints. One circle represents the average of a threefold measurement for the same NEP. The n_{efs} in the FMPS size range show that there were substantial differences among the different incinerated NEPs. The n_{efs} from incinerated paper ranged from 2.81×10^{12} to 3.22×10^{13} #/g and were in average greater than the n_{efs} from polymeric composites with values of 1.88×10^{12} to 5.54×10^{12} #/g and applied paints which ranged from 1.56×10^{11} to 4.16×10^{12} #/g (supplementary Table S2).

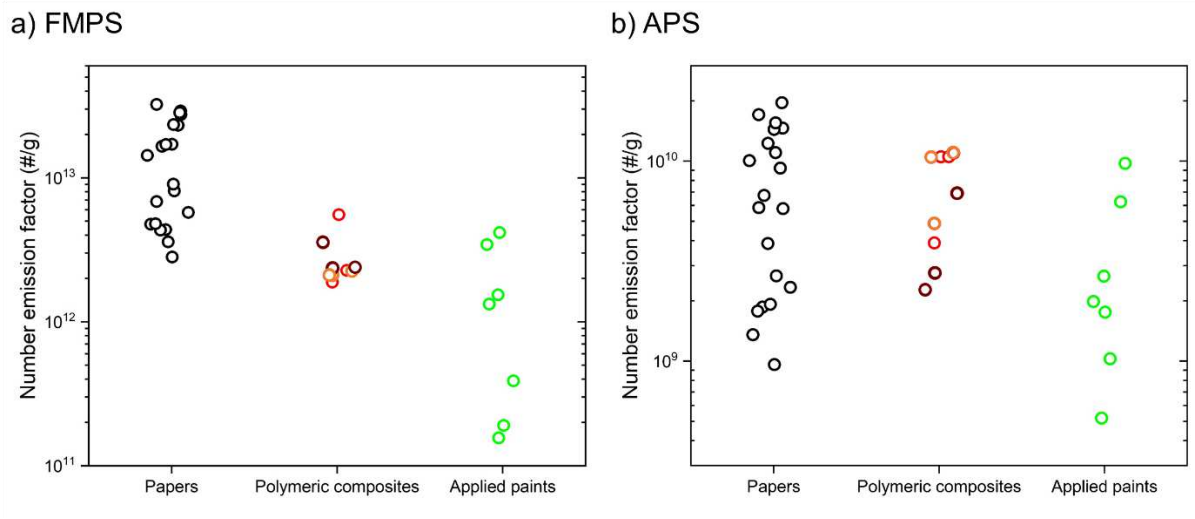

Fig. 2. Aerosol number emission factors (#/g) for aerosols from combusted paper with SiO_2 or Fe_2O_3 NMs, polymeric composites (TPU in orange, PA6 in dark red and PLA in red) with CuPhthalocyanine NMs and applied paints on spruce wood panels with SiO_2 or Fe_2O_3 NMs, a) in the FMPS size range of 5.6 nm – 560 nm and b) in the APS size range of 0.542 µm – 20 µm. One circle represents the average of a threefold measurement for the same NEP.

The n_{efs} for combusted paper, polymeric composite and applied paint in the APS size range were slightly smaller than those in the FMPS range and ranged from 9.61×10^{8} to 1.71×10^{10} #/g, 2.27×10^{9} to 1.10×10^{10} #/g and 5.19×10^{9} to 9.75×10^{9} #/g, respectively (supplementary Table S2). Higher NM loading in the NEP did not increase the n_{efs} in the FMPS range or in the APS range. The difference between the n_{efs} from any two types of NEPs was assessed via T-tests. Table S3 shows the compared categories with the resulting p-values and the respective significance. A smaller p-value implied a bigger difference between the two different categories of NEPs.

We noted substantial differences of the n_{efs} of paper, polymer composites and applied paints in the FMPS range (Table S3). The results implied that NEPs could be classified based on the n_{ef} in the FMPS range. The n_{efs} in the APS range did not show an obvious dependency on the type of the incinerated NEP.

3.2 Assessment of the released aerosol size distribution

The sizes of pristine NMs and released aerosols were compared to evaluate if pristine NMs were released in significant amount and to assess if the NMs were transformed. Pristine NMs had a maximum geometric size of 50 nm (supplementary Fig. S1 and supplementary Table S1) which could be detected in the electrical mobility size range.

Based on Hinds (1999) and DeCarlo et al. (2004), geometric size and electrical mobility size are similar for compact particles having a shape factor χ close to 1 and unit elementary charge. Except for the Fe_2O_3 nano rods, all other employed NMs (SiO_2, CuPhthalocyanine and Fe_2O_3 nano spheres) were compact or slightly elongated (and had a χ close to 1). For fibers, geometric size and electrical mobility size might differ significantly. In case of the short Fe_2O_3 nano rods with a geometric size of 8.4 ± 1.8 nm we calculated an electrical mobility diameter 7.01 ± 1.4 nm of using equation 4 and 5 from Bahk et al. (2013). Thus, the difference was actually rather small.

Table 1 shows the comparison of the sizes of the pristine NMs and the modes of the size distributions of the emitted aerosols. ASDs from PA6 and TPU showed a mode at around 30 nm, whereas the size distributions from PLA showed an additional mode at 102 nm. The ASDs did not show modes corresponding to the size of the pristine CuPhthalocyanine NM (14.6 ± 4.9 nm). The ASDs from "White paint 6.0 wt.% SiO_2" and the respective reference sample "Ref. white paint" showed two modes at around 30 nm and in size the range of 105 nm to 124 nm. No peak corresponding to the size of the silane-modified silica NM (12.0 ± 2.4 nm) was found. Similarly, there were two or three modes at about 30 nm, 55 nm, and in the range of 102 nm to 137 nm for red paint samples with Fe_2O_3 NMs. The ASDs did not show peaks at the electrical mobility diameter of 7.01 ± 1.4 nm that would indicate the presence of Fe_2O_3 nano rods. Free-standing Fe_2O_3 nano spheres with a diameter of 36.7 ± 12.4 nm might be part of the respective size distributions since there were modes at 30 nm and 55 nm. However, the size distributions of the reference sample also showed modes with these diameters. Released aerosols from paper

285 with silica, showed 2 to 4 modes in the range of 14 nm to about 103 nm. Although there was a
286 mode at 18 nm, the occurrence of this peak could not be linked to the emission of pristine silica
287 particles, which would appear at 14.0 ± 6.6 nm (silica std.) or 13.1 ± 2.3 nm (silica anis Al),
288 since the mode at 18 nm appeared also in the size distribution of the reference papers without
289 silica. Nevertheless, this peak was slightly higher when there were silica particles in the paper.
290 ASDs from paper with Fe_2O_3 NMs showed 2 to 4 modes in the size range of 18 nm to 110 nm
291 independent from the type of embedded NMs. All ASDs in the APS size range 0.542 µm to 20
292 µm showed modes at aerodynamic diameters of about 0.58 µm, 0.86 µm and 2.21 µm indicating
293 single pieces of matrix fragments with big diameters or aggregates and agglomerates of parti-
294 cles with smaller diameters.

295 **Table 1. Modes of aerosol size distributions from combusted polymeric composites with Cuphthalocyanine nano α and**
296 **Cuphthalocyanine nano β NMs, applied paints on spruce wood panels with SiO_2 and Fe_2O_3 NMs and paper with SiO_2**
297 **and Fe_2O_3 NMs in FMPS and APS size ranges compared to the geometric sizes of the pristine NMs.**

	Sample	*Size of released NMs in FMPS size range (nm)*				*Size of released NMs in APS size range (μm)*				*Size of pristine NMs (nm)*
Polymeric composites	PA6	28.1				0.62	0.89	2.04		
	PA6 α	26.5						2.00		14.6±4.9
	PA6 β	25.8				0.58	0.87	2.21		14.6±4.9
	PLA	27.5				0.9				
	PLA α	34.1	101.9			0.58	0.855	2.20		14.6±4.9
	PLA β	26.2	105.6			0.59	0.86	2.23		14.6±4.9
	TPU	34.3	102.1			0.58	0.89	2.10		
	TPU α	26.5				0.6				
	TPU β	27.3				0.58	0.86	2.02		14.6±4.9
Paints (applied on wood panels)	Ref. white paint	29.6			105.1	0.56	0.81	2.31		
	White paint 6.0 wt.% SiO_2	25.6			123.8	0.54	0.89	2.07		12.05±2.4
	Ref. for red paint	34.2			110.0	0.57	0.85	2.04		
	Red paint 7.0 wt.% Fe_2O_3 nano rods	29.8	101.9		118.7	0.55	0.85	2.10		8.4±1.8
	Red paint 7.0 wt.% Fe_2O_3 nano spheres	27.8	61.4			0.54	0.86	2.08		36.7±12.4
	Red paint 1.0 wt.% Fe_2O_3 nano rods	33.9	52.9		137.6	0.59	0.87	2.88		8.4±1.8
	Red paint 1.0 wt.% Fe_2O_3 nano spheres	35.3	55.1		123.5	0.58	0.84	2.03		36.7±12.4
Paper	Ref., no NM	16.2	19.7	34.9	96.7			1.69		
	Ref. , SiO_2 NM		19.3	40.0	99.7			1.69		
	Fe_2O_3 nano sphere, 0.05		22.4		96.8				2.18	36.7±12.4
	Fe_2O_3 nano sphere, 0.5		22.12		102.8			1.63		36.7±12.4
	Fe_2O_3 nano sphere, 5	18.1	21.8		99.2				2.02	36.7±12.4
	Fe_2O_3 nano rods, 0.05	16.2	21.9		98.7	0.64	0.92	1.23		8.4±1.8
	Fe_2O_3 nano rods, 0.5	17.1	22.8	30.1			1.07	1.69	1.86	8.4±1.8
	Fe_2O_3 nano rods, 5	17.6	25.8	34.4	97.6	0.69	0.89	1.46	1.86	8.4±1.8
	Commercial paper								2.22	
	Ref. no SiO_2	19.3	22.4	34.2				1.92	2.28	
	SiO_2 std., 0.8 (0.096 kg/t, active silica)	18.2		32.0	108.		0.84			14.0±6.6
	SiO_2 std., 3.0 (0.36 kg/t, active silica)	19.1		36.6			1.59	1.63		14.0±6.6
	SiO_2 std., 40 (4.8 kg/t, active silica)	18.1	25.0	30.7	96.8				2.12	14.0±6.6
	SiO_2 Al, 1.5 (0.105 kg/t, active silica)	19.0	23.0	34.7	44.4		0.85	1.66		14.0±6.6
	SiO_2 Al, 3.0 (0.21 kg/t, active silica)	16.4	19.9	38.6				1.72		14.0±6.6
	SiO_2 Al, 40 (2.8 kg/t, active silica)	14.4	18.5	32.6	40.7			1.92	2.28	14.0±6.6

3.3 Morphology assessment of aerosol particles

More than 200 SEM pictures were investigated to evaluate effects induced by the embedded NM, the matrix or the supporting structure (wood in case of applied paints) on the morphology of the fly ash particles. The SEM pictures showed particles with modified (irregular) shapes compared to the embedded NMs and their agglomerates (Fig. 3).

The number of particles on the filter depended on the mass of the burnt sample and the investigated location of the filters. Based on Fig. 3 we could not observe any noticeable effect by the type of embedded NMs nor the NM loading on the morphology of the released aerosols. If NM loadings would be higher than the range tested in this study (max. 7 wt.%), the NM loading could affect the morphology of the fly ash.

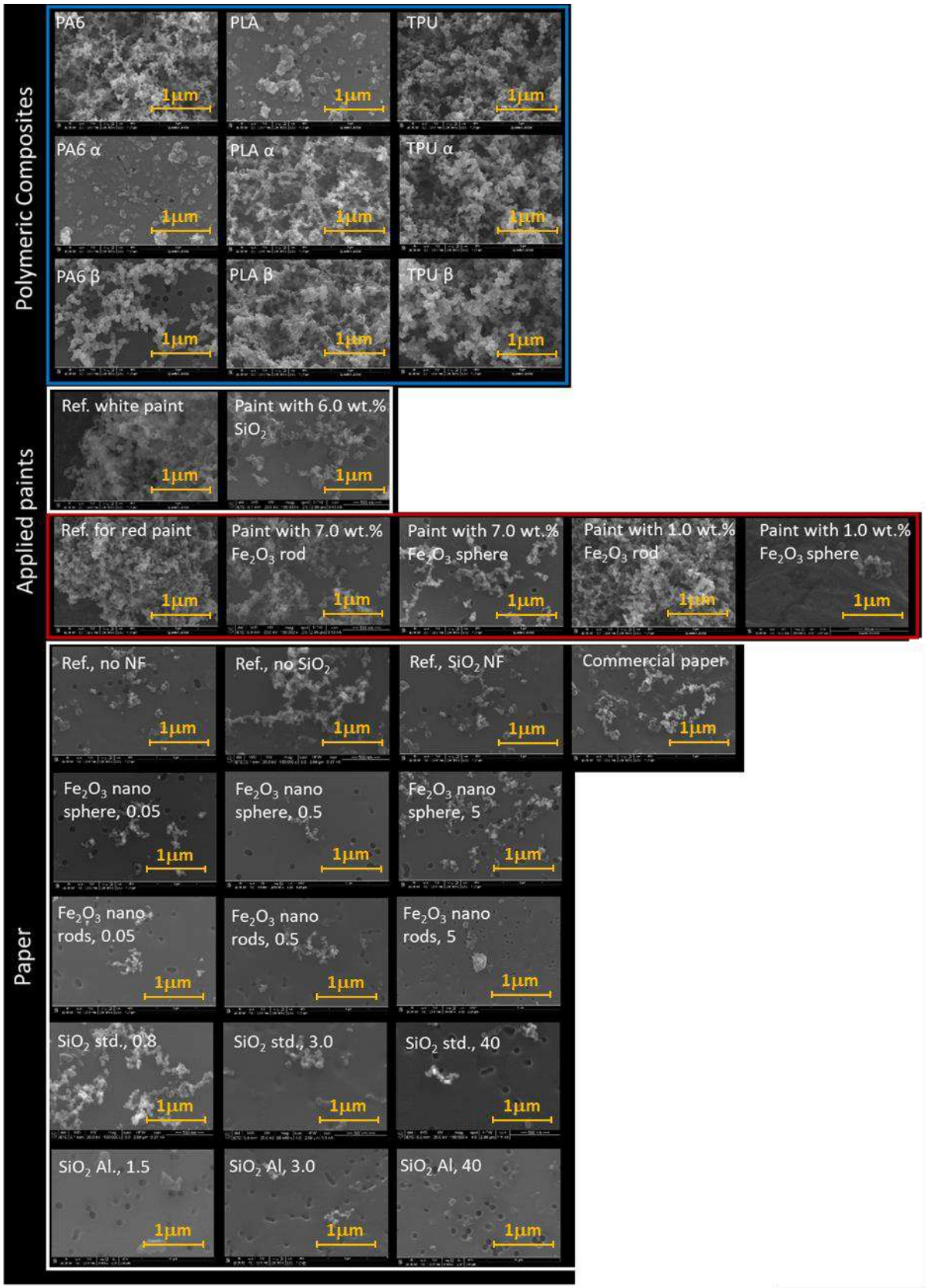

Fig. 3. SEM pictures of combustion-generated aerosols from polymeric composites with Cuphthalocyanine nano α and β, applied paints on wood panels with SiO_2 and Fe_2O_3 and paper with SiO_2 and Fe_2O_3.

3.4 Chemical characterization of the combustion-generated particles

3.4.1 Residual ash

The chemical composition of the residual ash was assessed via EDX-SEM (supplementary Tables S4-S6). The analyses showed high concentrations of chemical elements of the pristine NMs and other fillers of the NEPs. Residual ash from paper contained calcium, carbon and oxygen, which could be related to $CaCO_3$ fillers. Moreover, the detected silicon in the residual ash correlated with the silica loading in the NEP (supplementary Table S4) and the detected aluminum could be attributed to the polyaluminiumchloride component of the product formulation of the papers (see supplementary information). Fe from Fe_2O_3 in paper and Cu from CuPthalocyanine in polymeric composites could not be detected via EDX-SEM. Potentially Cu and Fe concentrations in the residual ash were below the detection limits of 0.02 % Cu and 0.03 % Fe of the EDX. Another reason could be that NMs deeply embedded in the matrix of the residual ash could potentially not be detected, since the X-rays from EDX analysis could not penetrate deep into the residual ash. The residual ash of the applied paints contained mainly elements from the embedded SiO_2, TiO_2 NMs in case of the white paint and Fe_2O_3 NMs in case of the red paint. Detected Si and Fe concentrations correlated with the NM loadings. The residual ash from "Paint with 7.0 wt.% Fe_2O_3 rods" showed a Fe-concentration of 20.7 % whereas the residual ash from "Paint with 1.0 wt.% Fe_2O_3 rods" showed a Fe-concentration of 2.4 %. This can be explained by a potential loss of carbon materials and the accumulation of non-volatile elements. Since the supporting wood panel comprised the majority of the mass of the paint NEPs, the residual elements coming from the wood also need to be considered. The low concentrations of Al and S could be attributed to the product formulation of the paint matrix. K, Ca, Mg, Na and partially also Si could be related to the so-called nutrients of the supporting spruce wood panels (Dünisch and Bauch 1994).

3.4.2 Released aerosols

Supplementary Table S7 depicts the results of the qualitative evaluation of the chemical composition of the fly ash via EDX-SEM. Accordingly, these particles consisted mainly of chemical

elements of the matrix (carbon, nitrogen, oxygen), oxygen from the air and in some cases marginal fractions of chemical elements (Cu and Si) which could be attributed to the NMs that were embedded in the NEPs. Fe from Fe_2O_3 and Si from SiO_2 could not be detected in the fly ash from the applied paints and paper with SiO_2 std. In contrast, low Si-concentrations correlating to the SiO_2 loadings in the paper could be detected in the fly ash from paper with embedded aluminum modified SiO_2. The detected platinum could be attributed to the platinum coating of the samples for SEM analyses. Details may be referred to supplementary Table S7.

Quantitative determination of the released signature elements of the embedded NMs was achieved via ICP-MS. Fig. 4 depicts the results. The release was calculated relative to the total mass of the fly ash deposited on the filter.

Fly ash from polymeric composites with CuPhthalocyanine NMs show Cu-concentrations in the range of 440 µg/g (PA6 β) to 20087 µg/g (PLA β). The crystalline phase of CuPhthalocyanine (α or β) NM did not strongly affect the Cu- concentration. In case of PLA and TPU, Cu from CuPhthalocyanine β was released in a higher amount. However, in case of PA6, the Cu-concentration from CuPhthalocyanine α was higher. PLA α released a lower Cu-concentration of 12569 µg/g than PLA β, which had a value of 20087 µg/g. PA6α, PA6β, TPUα and TPUβ released Cu-concentrations of 6820 µg/g, 440 µg/g, 658 µg/g and 4704 µg/g, respectively.

Fly ash from "White paint 6% SiO_2" did not show Si element. Fe was only detected for "Red paint 7.0% Fe_2O_3 rods" with a Fe-concentration of 2884 µg/g. The fly ash from the SiO_2-enhanced paper samples and the commercial paper did not show Si. Fly ash from paper with Fe_2O_3 NMs showed Fe-concentration of 936 µg/g in case of "Fe_2O_3 nano rods, 0.5". On the other hand, we did not detect Fe in the fly ash from the sample with the highest concentration of Fe_2O_3 nano rods ("Fe_2O_3 nano rods, 5"). Uncertainties in sampling and sample pretreatment might have influenced the detected concentrations of the Fe, Si and Cu signature elements.

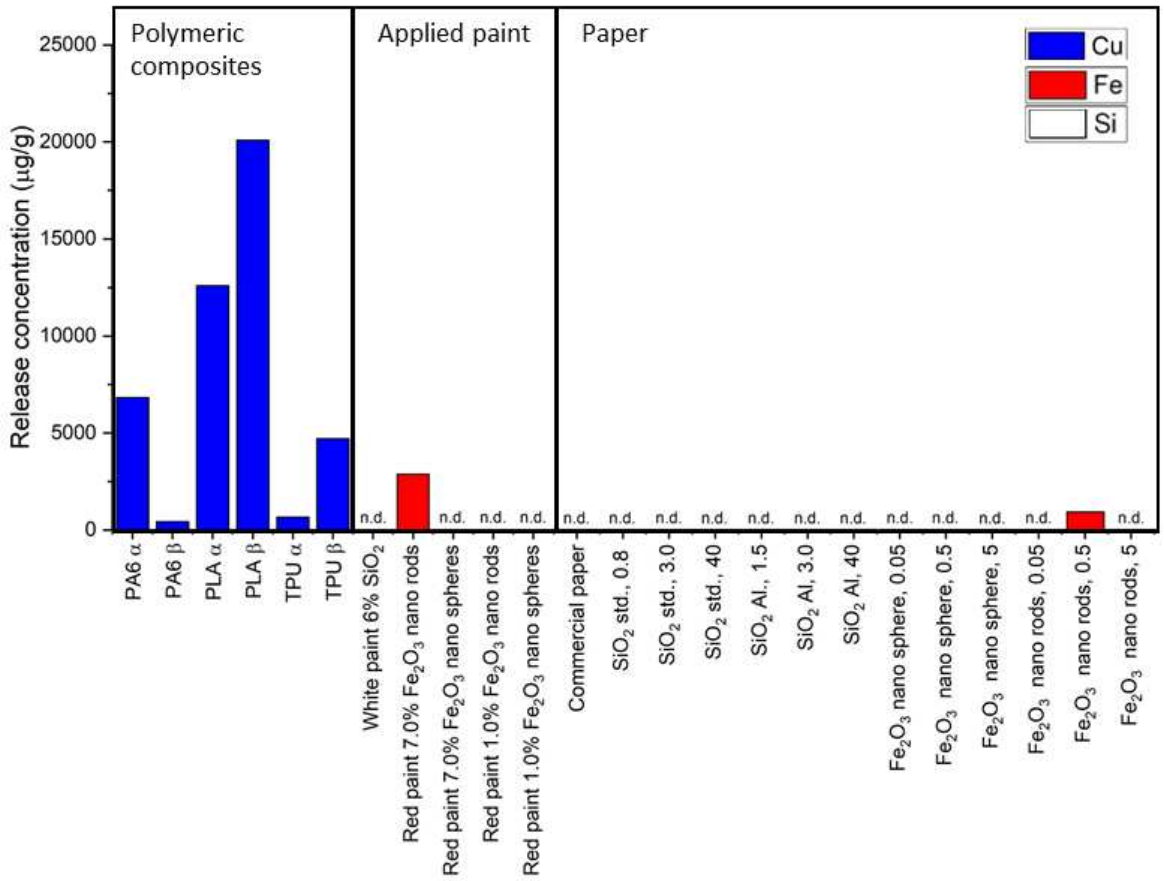

Fig. 4. Detected concentrations of Cu, Si and Fe signature elements of the embedded NMs in the aerosols from combusted polymeric composites with Cuphthalocyanine nano α and Cuphthalocyanine nano β and applied paints on wood panels with SiO_2 and Fe_2O_3 and paper with SiO_2 and Fe_2O_3. N.d. stands for not detected.

4. Discussion

Combustion of NEPs or waste with intentionally added NMs generates nanoparticles that are released either in form of fly ash or remain as a residue in form of solid ash (Part et al. 2018, Vejerano et al. 2014). According to Vejerano et al. (2014) and Part et al. (2018), the elements of the pristine NMs were sintered with other ash residues and accumulated in the residual ash after combustion. Only small fractions of the pristine NMs were released into the fly ash. According to Mueller et al. (2012), Mueller et al. (2013) and Part et al. (2018), the melting or boiling process of a NM and the bonding strength of the NM to the matrix defined its behavior during combustion. Based on their results, the probability for a NM to remain in the residual ash was higher when the NM was embedded in the matrix than if it was loosely attached to the surface of the matrix.

In this study, we explored the NM release from NEPs with embedded NMs. We compared experimental data from the combustion-generated particles of multiple NEPs to evaluate the NM release potential and to assess how pristine NM and matrix influence size, shape and chemical composition of the fly ash. In case the melting point of the NM was above the combustion temperature, we expected NMs accumulating in the residual ash and did not exclude the presence of pristine NMs in the fly ash. However, even at combustion temperatures that are lower than the melting points, the generated heat could induce modification of the pristine NMs, which then could lose their integrity. As described by Part et al. (2018) the vaporized material including generated elements and fragments might recombine / re-condense in the flue gas, which then would affect the shape or chemical composition of the newly generated nanoparticles. We expect that SiO_2 and Fe_2O_3 NMs were not melted, since they have melting points of 1600°C (Chemical Abstracts Service (CAS) no. 7631-86-9) and 1565 °C (CAS no. 1309-37-1), respectively, which indicates that they remained in the residual ash. At elevated temperatures (already below 500°C), colloidal silica particles start to sinter to a very low surface area (outside the nano range). All particles would be fully sintered at a temperature of about 900°C. In addition, the size of the elongated (anisotropic) silica structures was changed during the sintering process.

The efficacy of the sintering process increases due to the presence of Na counter ions. Since Silica anis std and Silica anis Al had a high content of Na. Due to their high surface area, they sintered even more compared to other amorphous silicas. Moreover, due to the sintering, the anisotropic structure and the size of the particles was very different after the combustion.

In contrast the CuPhthalocyanine NMs could be totally destroyed during the combustion, due to their melting point of 150°C (CAS no. 147-14-8).

We detected aerosol release in the nano size range for all NEPs combusted. The total released aerosol concentrations from polymeric composites, paints and paper were quite different.

To assess these differences, we compared the n_{efs} for the different NEPs. The n_{efs} for aerosols in the FMPS size range revealed substantial differences among different NEPs (Table S2 and Table S3). Differences in this size range were expected since the release of nanosized particles during the combustion depends strongly on the type of NEP that was combusted. The n_{efs} of combusted paper ranging from 2.81×10^{12} to 3.22×10^{13} #/g were on average greater than the n_{efs} of polymeric composites (1.88×10^{12} to 5.54×10^{12} #/g) and much greater than the n_{efs} of applied paints (1.56×10^{11} to 4.16×10^{12} #/g). The difference in the n_{efs} in the FMPS range implied that the type of NEP/ matrix (paper, polymer composite or paint on wood panels) could be the determining factor for the aerosol concentration. The difference among the n_{efs} in the APS size range was not significant for the different types of NEPs (Table S2 and Table S3). The results from the T-tests on n_{efs} in the FMPS range implied that different NEPs could be categorized based on the n_{ef} in the FMPS range, which corresponded to the potential of the NEP to release aerosols during combustion. Thus, we defined three categories polymeric composites, applied paints and paper. Referring to Table S2, we conclude that there was no correlation between the NM loading of the NEPs and the aerosol number emission factor.

However, there are limitations of the FMPS instrument that need to be taken into account. Several studies reported that particles in unipolar diffusion chargers were wrongly sized in the upper working size ranges (Price et al. 2014, Fonseca et al. 2016, Levin et al. 2015, Zimmermann et al. 2015). Based on Price et al. (2014), FMPS measurements detected to some extent lower concentrations at an electrical mobility diameter of 110 nm compared to the scanning mobility particle sizer that showed a higher accuracy compared to FMPS. The lower accuracy of the FMPS might have affected the detected aerosol concentration.

Since the matrix comprised the major part of the NEP used in this study, the type of matrix drove the amount of generated nanoparticles whereas the embedded amount of NMs did not strongly influence the amount of generated nanoparticles. We suppose that if the NM loading in the NEP would be significantly higher, it could affect the concentration of generated aerosols.

For the case of pigments, the tested NEPs are intensely colored (Table S1), confirming that the tested concentrations of NM cover the industrially relevant range for pigments.

Since total aerosol concentrations from samples with NMs were not remarkably different compared to those from reference samples without NMs, we could not conclude a specific influence of adding NMs to composite matrices on the total aerosol concentrations. This goes along with the findings of Vejerano et al. (2014) who found that the particle emission factor of surrogate waste from polymers was not significantly increased due to the presence of NMs.

To assess the generation of new particles during the combustion and to evaluate the release of pristine NMs we compared the geometric sizes of the pristine NMs with the modes of the released ASDs. The ASDs from paints and polymers showed a dominant mode at about 30 nm and a minor mode at about 100 nm whereas the ASDs from paper showed small modes at about 17 nm and 20 nm, which sometimes replaced the mode at 30nm. The sizes of the detected modes in the aerosol did not correspond to the sizes of the pristine NMs that were embedded in the NEPs. If CuPhthalocyanine, SiO_2 or Fe_2O_3 were released in significant amount in pristine form, there would be modes with the sizes of the pristine NMs.

Nonetheless, this does not mean that the embedded NMs were not released, because if they were released in very little amount, the size of the pristine NM could not be seen on the ASDs.

The ASDs from all NEPs showed multiple modes in the APS range, indicating big particles (e.g. matrix fragments) or agglomerates of smaller particles. The underlying self-aggregation mechanism for combustion-generated aerosols was described by Forster et al. (2016). Many particles in the fly ash showed different morphologies from pristine NMs and had an irregular shape. However, we could not conclude that all particles had a different morphology from the pristine NMs since some particles might be hidden behind other particles in the SEM images.

The EDX-SEM analysis of the fly ash showed mainly chemical elements of the matrices used.

In the case of paper, EDX-SEM analysis showed high amount of $CaCO_3$ (Table S4) which was apart from the small content of silica and Fe_2O_3 a major part of the product formulation of the paper (Table S1). In some cases, marginal amounts of chemical elements were found that could be related to the pristine NMs. This correlates with the results from Vejerano et al. (2014) and Vejerano et al. (2013), who investigated the combustion of plastic and paper wastes that contained different kinds of NMs (TiO_2, CeO_2, Ag, Fe_2O_3, etc.) using a combustion temperature of 850 °C. Their results implied that the majority of NMs remained in the residual ash whereas only a small amount of the pristine NMs was released in form of fly ash.

ICP-MS determination of the released concentrations of Cu, Si, Fe signature elements of the NMs in the fly ash showed substantial differences. PLA released more copper than PA6 and TPU among the polymeric composites. Thus, the type of matrix affected the Cu-concentration in the fly ash. In addition, the behavior of the NM influenced the concentration of the released signature elements. The copper concentration in the fly ash from polymeric composites was in comparison much higher than the concentrations of Si and Fe in paint and paper samples that contained SiO_2 and Fe_2O_3.

A reason could be that the SiO_2 and Fe_2O_3 NM were not melted due to their melting points of 1600°C and 1565 °C, which thereby reduced the concentration of the signature elements in the fly ash. Another reason, why no significant release of Si could be detected in the fly ash could be the sintering of the colloidal silica particles, which increased the probability of the Si to remain in the residual ash and thereby reduced the probability of Si in the fly ash. In contrast, the pristine CuPhthalocyanine NMs were melted due to their melting point of 150°C and released in higher amounts.

In case of paint and paper, little amount of Fe was detected in the fly ash from the red paint with 7.0 wt.% Fe_2O_3 nano rods and from the paper with 0.05% Fe_2O_3 nano rods. With a length of 8.4 ± 1.8 nm, rod-shaped Fe_2O_3 NMs had a smaller geometric size than the spherical NMs

that had a diameter of 36.7 ± 12.4 nm. Iron was only detected for NEPs with rod-shaped Fe_2O_3 NMs, but not for the NEPs with spherical Fe_2O_3 NMs. This implied that shape and size of the Fe_2O_3 NM affected the Fe-concentration in the fly ash particles. However, the data were too limited for a definite conclusion. The detected Si-values in the fly ash from the paper and paint samples with silica were similar to the blank values of the Nuclepore filter. Thus, the Si amount was not significant. Sampling or pretreatment issues or very low concentrations of Fe and Si that were below the detection limits and differences of the LODs, which depended on the sample mass, could have affected the results and might limit the evaluation of the concentrations of the Fe and Si signature elements in the fly ash.

Similarly, Singh et al. (2019) who investigated incineration-induced NM release for acryl-based polymer composites with SiO_2, Fe_2O_3 and CuO NMs in various loading from 0.3 to 20 wt.% could not detect Si in the released aerosol. Only Fe or Cu could be detected. Haynes et al. (1982) showed that a small fraction of refractory oxides (CaO, MgO, SiO_2, Fe_2O_3) was reduced to volatile sub oxides or elements, which diffused away from the burning particle. Since the temperature used for the combustion (570°C) was lower than 1750°C above which SiO_2 particles would become volatile, volatile SiO_2 particles were not expected to occur.

Results from Singh et al. (2019) who applied various NM loadings in the range of 0.3 to 20 wt.%, implied that higher NM loadings in the NEPs, could be linked to higher concentrations of the signature elements of the respective NMs in the fly ash. The results from this study did not show such a trend. The reason could be that the NM loadings in the real-world NEPs that were used in this study were smaller.

The EDX analysis of the residual ash from the samples that were burnt in this study showed high concentrations of chemical elements of the embedded NMs, which implied that high fractions of the NMs, which were embedded in the NEP, remained in the residual ash.

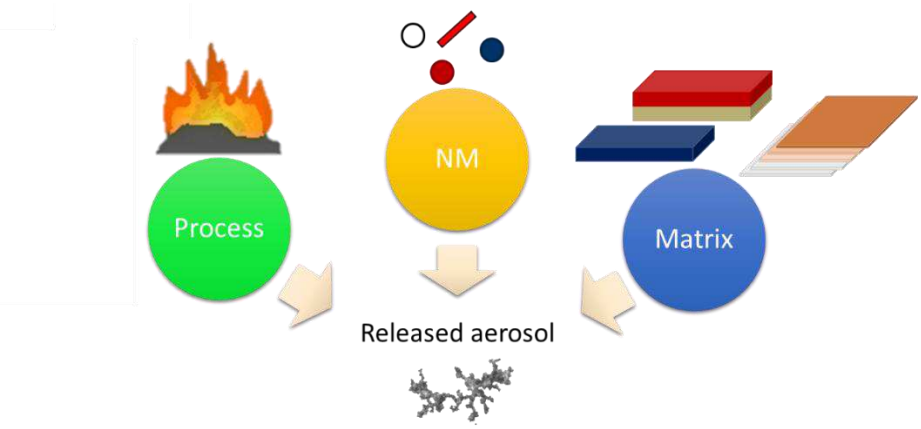

Fig. 5. Graphic showing the influence of process, nanomaterial (NM) and matrix on the released aerosol.

5 Conclusion

We assessed the influence of the type of matrix and the type of pristine NM on the concentration and the chemical composition of combustion-generated aerosols from real-world NEPs such as paint, polymeric composites and paper with SiO_2, Fe_2O_3 and CuPhthalocyanine NMs. The combustion conditions were intentionally different from the legally required conditions of waste incineration. Physical-chemical characterization of the fly ash showed particles with modified chemical composition and transformed size as compared to the pristine NMs. The fly ash particles gained their chemical composition mainly from the matrix and only to a minor fraction from type the pristine NMs.

Considering aerosol concentrations, n_{efs}, concentrations of released signature elements and morphologies of the released particles, we conclude that the physical-chemical characteristics of the combustion-generated fly ash from the NEPs, that were used in this study, were simultaneously influenced by the matrix type, the properties of the pristine NM and by the process (combustion) (Fig. 5). The calculated n_{efs} in the FMPS range depended on the type of NEP, which implied that the NEPs could be categorized according to their potential to release aerosols when they were burnt. It turned out that the embedded NMs did not strongly affect this release potential. The results facilitate grouping and read-across of NEPs and NMs with similar hazard profiles.

Albeit there were only low concentrations of chemical elements of the pristine NMs in the fly ash, these particles - regardless of their origin from burning conventional materials or NEPs - might lead to adverse health effects if they are inhaled into the alveoli and trachea bronchus of the lung. The generated data facilitates a comprehensive risk assessment of NEP.

Acknowledgement

The authors thank Dr. Davide Bleiner for his support and for providing the lab equipment for the chemical analyses of the fly ash.

Conficts of interest

The authors do not declaim any financial interests.

Funding

This study was financed by the European project GRACIOUS (project number: 760840).

References

Bahk Y. K., Buha J. and Jing Wang (2013): Determination of Geometrical Length of Airborne Carbon Nanotubes by Electron Microscopy, Model Calculation, and Filtration Method, Aerosol Science and Technology, 47:7, 776-784, Doi.:10.1080/02786826.2013.791745

Basinas I, Sánchez Jiménez A, Galea KS, van Tongere M, Hurley F (2018), A systematic review of the routes and forms of exposure to engineered nanomaterials. Ann Work Expo Health, 62: 639–662

Bello D., Martin J., Santeufemio C., Sun Q., Bunker K. L., S. M. & Demokritou P. (2013) Physicochemical and morphological characterisation of nanoparticles from photocopiers: implications for environmental health, Nanotoxicology, 7:5, 989-1003, DOI: 10.3109/17435390.2012.689883

Brar S. K., Verma M., Tyagi R.D, Surampalli R.Y. (2010). Engineered nanoparticles in wastewater and wastewater sludge – Evidence and impacts, Waste Management, Volume 30, Issue 3, pages 504-520, doi.org: /10.1016/j.wasman.2009.10.012.

Breuer O, Sundararaj U (2004) Big returns from small fibers: A review of polymer/carbon nanotube composites. Polym Compos 25:630–645. https://doi.org/10.1002/pc.20058

Buha J., Mueller N., Nowack B., Ulrich A., Losert S., and Wang J. (2014) Physical and Chemical Characterization of Fly Ashes from Swiss Waste Incineration Plants and Determination of the Ash Fraction in the Nanometer Range, Environmental Science & Technology 48 (9), 4765-4773, DOI: 10.1021/es4047582

555 Chemical Abstracts Service: CuPhthalocyanine: CAS no. 147-14-8, SiO2: CAS no. 7631-86-
556 9, Fe2O3 CAS no 1309-37-1, https://www.cas.org/
557 Chivas-Joly C. et al., (2014) “Influence of carbon nanotubes on fire behaviour and aerosol
558 emitted during combustion of thermoplastics,” Fire Mater., vol. 38, no. 1, pp. 46–62.
559 Chivas-Joly C., Longuet C., Pourchez J., Leclerc L., Sarry G.,. Lopez-Cuesta J.-M, “Physical,
560 morphological and chemical modification of Al-based nanofillers in by-products of incin-
561 erated nanocomposites and related biological outcome,” J. Hazard. Mater., vol. 365, no.
562 September 2018, pp. 405–412, Mar. 2019.
563 DeCarlo P. F., Slowik J. G., Worsnop D. R., Davidovits P., Jimenez J. L. (2004) Particle Mor-
564 phology and Density Characterization byCombined Mobility and Aerodynamic Diameter-
565 Measurements. Part 1: Theory Aerosol Science and Technology,38:1185–1205, DOI:
566 10.1080/027868290903907
567 Dünisch, O., & Bauch, J. (1994). Influence of Mineral Elements on Wood Formation of Old
568 Growth Spruce (Picea abies [L.] Karst.), Holzforschung, 48(s1), 5-14. doi:
569 https://doi.org/10.1515/hfsg.1994.48.s1.5
570 Froggett SJ, Clancy SF, Boverhof DR et al. (2014) A review and perspective of existing re-
571 search on the release of nanomaterials from solid nanocomposites. Part Fibre Toxicol 11:
572 17. doi: 10.1186/1743-8977-11-17
573 Fonseca A.S., Viana M., Pérez N., Alastuey A., Querol X., Kaminski H., Todea A. M., Monz
574 C. & Asbach C. (2016) Intercomparison of a portable and two stationary mobility particle
575 sizers for nanoscale aerosol measurements, Aerosol Science and Technology, 50:7, 653-
576 668, DOI: 10.1080/02786826.2016.1174329
577 Gonçalves Carolina, Gonçalves Inês C., Magalhães Fernão D., Pinto Artur M. (2018)
578 Poly(lactic acid) Composites Containing Carbon-Based Nanomaterials: A Review. MDPI
579 Haynes B. S, Neville M., Quann R. J., Sarofim A. F., (1982) Factors governing the surface
580 enrichment of fly ash in volatile trace species, Journal of Colloid and Interface Science,
581 87, 1, 266-278, 0021-9797, DOI:10.1016/0021-9797(82)90388-5.
582 Hammer, T., Gao, H., Pan, Z. and Wang, J. (2020). Relationship between Aerosols Exposure
583 and Lung Deposition Dose. Aerosol Air Qual. Res. 20: 1083-1093.
584 https://doi.org/10.4209/aaqr.2020.01.0033
585 Hansen, S. F., Hartmann, N. B., & Baun, A. (2015). Transformation and distribution pro-
586 cesses governing the Fate and behaviour of nanomaterials in the environment: an over-
587 view. In Sustainable Nanotechnology Conference 2015: Conference abstracts Venice, It-
588 aly.
589 Hinds WC. Aerosol technology: properties, behavior and measurement of airborne particles.
590 New York: Wiley-Interscience; 1999.
591 Keller A. and Lazareva A. (2014), Predicted Releases of Engineered Nanomaterials: From
592 Global to Regional to Local Environ. Sci. Technol. Lett., 1, 65–70. DOI:
593 10.1021/ez400106t
594 Kittelson D.B., Watts W.F., Johnson J.P. (2004), Nanoparticle emissions on Minnesota high-
595 ways, Atmospheric Environment, Volume 38, Issue 1, , Pages 9-19, doi:/10.1016/j.at-
596 mosenv.2003.09.037.

Kotnarowska D., Przerwa M. and Szumiata T. Resistance to Erosive Wear of Epoxy-Polyurethane Coating Modified With Nanofillers Journal of Materials Science Research; Vol. 3, No. 2; 2014 doi:10.5539/jmsr.v3n2p52

Kuhlbusch, T.A., Fissan, H. and Asbach, C. (2010). Measurement and Detection of Nanoparticles Within the Environment. In Nanotechnology, (Ed.). doi:10.1002/9783527628155.nanotech017

Landsiedel, R., 2016. Concern-driven integrated approaches for the grouping, testing andassessment of nanomaterials. Environ. Pollut. 218, 1376–1380.

Le J-L, Du H, Pang SD (2014). Use of 2D Graphene Nanoplatelets (GNP) in cement composites for structural health evaluation. Composites Part B: Engineering 67:555–563. https://doi.org/10.1016/j.compositesb.2014.08.005

Levin, M., Gudmundsson, A., Pagels, J. H., Fierz, M., Mølhave, K., L€ondahl, J., Jensen, K. A., Koponen, I. K. (2015). Limitations in the use of Unipolar Charging for Electrical Mobility Sizing Instruments: A Study of the Fast Mobility Particle Sizer. Aerosol Sci. Technol., 49(8):556–565. doi: 10.1080/ 02786826.2015.1052039

Limited, R. E.-S. P. (2011). Nanotechnology Market Forecast to 2013. RNCOS E-Services Private. Hazard assessment of nanomaterials in consumer products

Madkour L.H. (2019) Introduction to Nanotechnology (NT) and Nanomaterials (NMs). In: Nanoelectronic Materials. Advanced Structured Materials, vol 116. Springer, Cham. https://doi.org/10.1007/978-3-030-21621-4_1

Mahrholz T., Stängle J., Sinapius M., (2009) Quantitation of the reinforcement effect of silica nanoparticles in epoxy resins used in liquid composite moulding processes, Composites Part A: Applied Science and Manufacturing, Volume 40, Issue 3, Pages 235-243

Massari A., Beggio M., Hreglich S., Marin R., Zuin S, (2014) Behavior of TiO2 nanoparticles during incineration of solid paint waste: A lab-scale test, Waste Management, 34, 10, 1897-1907, ISSN 0956-053X, Doi: 10.1016/j.wasman.2014.05.015.

Ministère de l'Environnement, d. l. É. e. d. l. M., (2015) Éléments issus des déclarations des substances à l'état nanoparticulaire: Exercice 2015.

Mitrano D. M., Motellier S., Clavaguera S., Nowack B. (2015), Review of nanomaterial aging and transformations through the life cycle of nano-enhanced products, Environment International, Volume 77, Pages 132-147, ISSN 0160-4120, https://doi.org/10.1016/j.envint.2015.01.013.

Mueller N.C., Buha J., Wang J., Ulrich A. and Nowack B. (2013) Modeling the flows of engineered nanomaterials during waste handling, Environ. Sci.: Processes Impacts, 15, 251-259, DOI: 10.1039/C2EM30761H.

Mueller, N. C.; Nowack, B.; Wang, J.; Ulrich, A.; Buha, J. (2012). Nanomaterials in waste incineration and landfills. Internal Empa-report, Empa-Swiss Federal Laboratories for Materials Science and Technology.

Nowack B and Bucheli TD (2007) Occurrence, behavior and effects of nanoparticles in the environment. Environ Pollut 150:5–22. https://doi.org/10.1016/j.envpol.2007.06.006

Nowack, B; Ranville, James F.; Diamond, Stephen; Gallego-Urrea, Julian A.; Metcalfe, Chris; Rose, Jerome et al. (2012): Potential scenarios for nanomaterial release and subsequent alteration in the environment. In: Environmental toxicology and chemistry 31 (1), S. 50–59. DOI: 10.1002/etc.726.

Oischinger, J., Meiller, M., Daschner, R., Hornung, A., & Warnecke, R. (2019). Fate of nano titanium dioxide during combustion of engineered nanomaterial-containing waste in a municipal solid waste incineration plant. Waste Management & Research, 37(10), 1033–1042. https://doi.org/10.1177/0734242X19862603

Oomen, A.G.; Bleeker, E.A.J.; Bos, P.M.J.; Van Broekhuizen, F.; Gottardo, S.; Groenewold, M.; Hristozov, D.; Hund-Rinke, K.; Irfan, M.-A.; Marcomini, A.; Peijnenburg, W.J.G.M.; Rasmussen, K.; Jiménez, A.S.; Scott-Fordsmand, J.J.; Van Tongeren, M.; Wiench, K.; Wohlleben, W.; Landsiedel, R. (2015) Grouping and Read-Across Approaches for Risk Assessment of Nanomaterials. Int. J. Environ. Res. Public Health, 12, 13415-13434.

Part F., Berge N., Baran P., Stringfellow A., Sun W., Bartelt-Hunt S., Mitrano D., Li L., Hennebert P., Quicker P., C. Bolyard S., Huber-Humer M.. (2018) A review of the fate of engineered nanomaterials in municipal solid waste streams, Waste Management, Volume 75, Pages 427-449, ISSN 0956-053X, https://doi.org/10.1016/j.wasman.2018.02.012.

Pope, C. A., III; Dockery, D. W.; Schwartz, J. (1995) Review of epidemiological evidence of health effects of particulate air pollution. Inhalation Toxicol., 7, 1-18.

Potts JR, Dreyer DR, Bielawski CW, Ruoff RS (2011) Graphene-based polymer nanocomposites. Polymer 52:5–25. https://doi.org/10.1016/j.polymer.2010.11.042

Price, H. D., Stahlmecke, B., Arthur, R., Kaminski, H., Lindermann, J., Däuber, E., Asbach, C., Kuhlbusch, T. A. J., BéruBé, K. A., Jones, T. P. (2014), Comparison of Instruments for Particle Number Size Distribution Measurements in Air Quality Monitoring. J. Aerosol Sci., 76(0):48–55. doi:10.1016/j.jaerosci.2014.05.001

Roes, L., Patel, M.K., Worrell, E., Ludwig, C., 2012. Preliminary evaluation of risks related to waste incineration of polymer nanocomposites. Sci. Total Environ. 417, 76–86.

Rothen-Rutishauser B. M., Schürch S., Haenni B., Kapp N. and Gehr Peter (2006) Interaction of Fine Particles and Nanoparticles with Red Blood Cells Visualized with Advanced Microscopic Techniques Environmental Science & Technology 40(14),4353-4359 DOI: 10.1021/es0522635

Ruggiero, E.; Vilsmeier, K.; Mueller, P.; Pulbere, S.; Wohlleben, W., (2019) Environmental release from automotive coatings are similar for different (nano)forms of pigments. Environmental Science: Nano, 6 (10), 3039-3048.

Schlagenhauf, L., Kuo, Y., Bahk, Y.K. et al. Decomposition and particle release of a carbon nanotube/epoxy nanocomposite at elevated temperatures. J Nanopart Res 17, 440 (2015). https://doi.org/10.1007/s11051-015-3245-5

Schulz, H.; Harder, V.; Ibald-Mulli, A,; Khandoga, A.; Koenig, W.; Krombach, F.; Radykewicz, R.; Stampfl, A.; Thorand, B.; Peters, A. (2005) Cardiovascular effects of fine and ultrafine particles. J. Aerosol Med., 18, 1-22.

677 Seipenbusch M, Mingzhou Y, Asbach C, Kuhlbusch TAJ, Lidé G. (2014) From Source to
678 Dose: Emission, Transport, Aerosol Dynamics and Dose Assessment for Workplace Aero-
679 sol Exposure. In: Handbook of Nanosafety – Measurement, Exposure and Toxicology,
680 (Vogel U. eds.). Academic Press, Elsevier, Amsterdam, Netherlands, pp. 135–71.
681 Singh D., Schifman L. A., Watson-Wright C., Sotiriou G. A., Oyanedel-Craver V., Wohlleben
682 W., and Demokritou P. (2017). Nanofiller Presence Enhances Polycyclic Aromatic Hy-
683 drocarbon (PAH) Profile on Nanoparticles Released during Thermal Decomposition of
684 Nano-enabled Thermoplastics: Potential Environmental Health Implications, Environmen-
685 tal Science & Technology 51 (9), 5222-5232, DOI: 10.1021/acs.est.6b06448
686 Singh D., Wohlleben W., De La Torre Roche R., White J. C, Demokritou P., (2019) "Thermal
687 decomposition/incineration of nano-enabled coatings and effects of nanofiller/matrix
688 properties and operational conditions on byproduct release dynamics: Potential environ-
689 mental health implications," NanoImpact, vol. 13, no. September, pp. 44–55, 2019.
690 Singh, D., Sotiriou, G.A., Zhang, F., Mead, J., Bello, D., Wohlleben, W., Demokritou, P.,
691 (2016). End-of-life thermal decomposition of nano-enabled polymers: effect of nanofiller-
692 loading and polymer matrix on byproducts. Environ. Sci. Nano 3 (6), 1293–1305.
693 Sotiriou G. A., Singh D., Zhang F., Chalbot M.-C. G., Spielman-Sun E., Hoering L., Ka-
694 vouras I. G., Lowry G. V., Wohlleben W., Demokritou P., (2016). Thermal decomposition
695 of nano-enabled thermoplastics: Possible environmental health and safety implications,
696 Journal of Hazardous Materials, Volume 305, Pages 87-95, ISSN 0304-3894,
697 DOI:10.1016/j.jhazmat.2015.11.001.
698 Sotiriou G. A., Singh D., Zhang F., Wohlleben W., Chalbot M.-C. G., Kavouras I. G. and
699 Demokritou P. (2015), An integrated methodology for the assessment of environmental
700 health implications during thermal decomposition of nano-enabled products Environ. Sci.:
701 Nano, 2015,2, 262-272 DOI:10.1039/C4EN00210E
702 Sow C., Riedl B., Blanchet P., UV-waterborne polyurethane-acrylate nanocomposite coatings
703 containing alumina and silica nanoparticles for wood: mechanical, optical, and thermal
704 properties assessment J. Coat. Technol. Res., 8 (2) 211–221, 2011 DOI 10.1007/s11998-
705 010-9298-6
706 Stahlmecke, B. Asback C. Todea A, Kaminski H. Kuhlbusch T. A. J. (2014) In book: HAND-
707 BOOK OF NANOSAFETY MEASUREMENT, EXPOSURE AND TOXICOLOGY
708 Chapter: 7.4 Investigations on CNT Release from Composite Materials During End of
709 Life
710 Surendhiran, D., Cui, H. and Lin, L. (2020). Mode of Transfer, Toxicity and Negative Impacts
711 of Engineered Nanoparticles on Environment, Human and Animal Health. In The ELSI
712 Handbook of Nanotechnology, C.M. Hussain (Ed.). doi:10.1002/9781119592990.ch9
713 Vejerano, E. P.; Holder, A. L.; Marr, L. C. (2013). Emissions of Polycyclic Aromatic Hydro-
714 carbons, 1645Polychlorinated Dibenzo-p-Dioxins, and Dibenzofurans from Incineration
715 of Nanomaterials. Environmental 1646Science & Technology 47(9): 4866-4874.
716 Vejerano, E.P., Leon, E.C., Holder, A.L., Marr, L.C., (2014). Characterization of particle
717 emissions and fate of nanomaterials during incineration. Environ. Sci. Nano 1 (2), 133–
718 143.

719 Walser, T., Limbach, L., Brogioli, R. et al. (2012) Persistence of engineered nanoparticles in a
720 municipal solid-waste incineration plant. Nature Nanotech 7, 520–524
721 https://doi.org/10.1038/nnano.2012.64
722 Wang J., Schlagenhauf L., Setyan A., "Transformation of the released asbestos, carbon fibers
723 and carbon nanotubes from composite materials and the changes of their potential health
724 impacts," J. Nanobiotechnology, vol. 15, no. 1, p. 15, 2017
725 Watson-Wright, C., Singh, D., Demokritou, P., 2017. Toxicological implications of released
726 particulate matter during thermal decomposition of nano-enabled thermoplastics. NanoIm-
727 pact 5, 29–40.
728 Wigger H., Wohlleben W. and Nowack B. (2018), Redefining environmental nanomaterial
729 flows: Consequences of the regulatory nanomaterial definition on the results of environ-
730 mental exposure models, Environ. Sci.: Nano, 5, 1372–1385.
731 Zimmerman, N., Jeong, C.-H., Wang, J. M., Ramos, M., Wallace, J. S., Evans,G. J.(2015), A
732 Source-independent Empirical Correction Procedure for the Fast Mobility and Engine Ex-
733 haust Particle Sizers. Atmo. Environ. 100:178–184. doi: http://dx.doi.org/10.1016/j.at-
734 mosenv. 2014.10.054

Figures

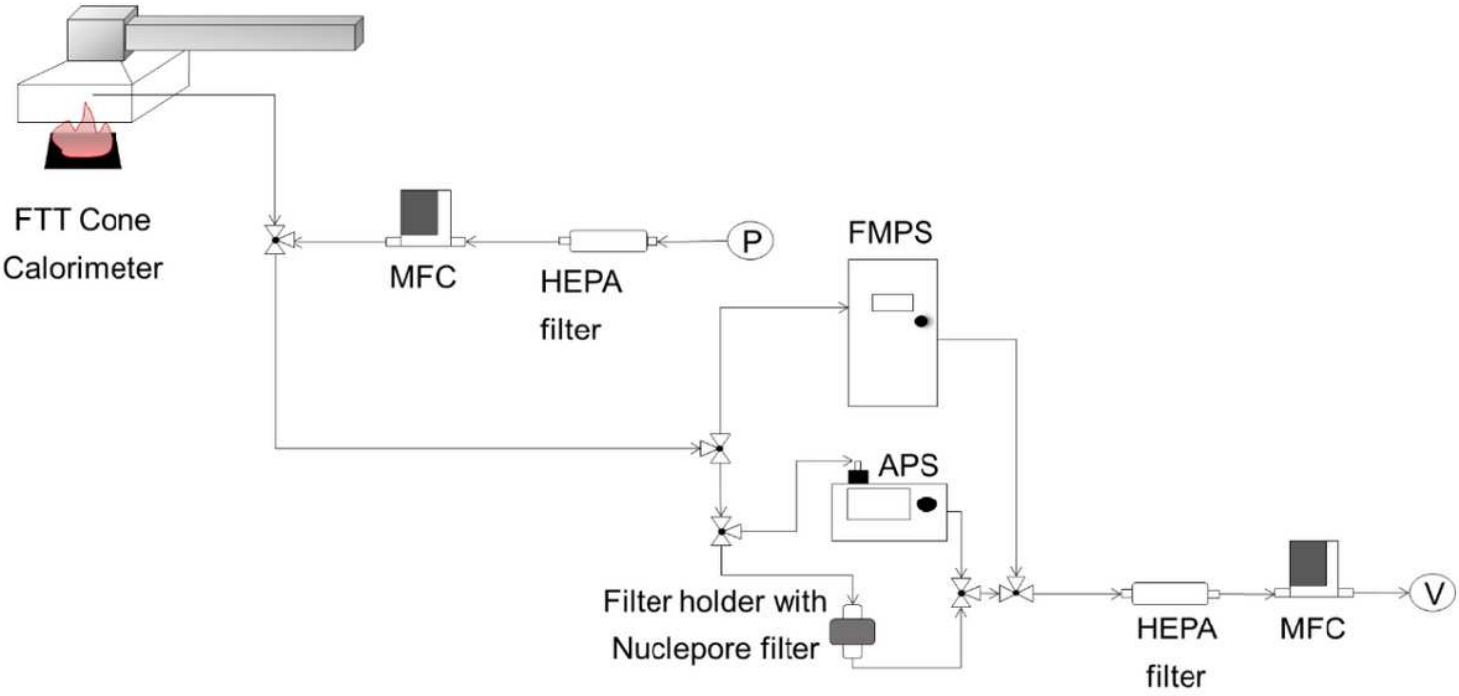

Figure 1

Setup used for combustion experiments, aerosol measurement and fly ash collection with Cone Calorimeter (FTT), mass flow controllers (MFCs), HEPA filters, fast mobility particle sizer (FMPS), aerodynamic particle sizer (APS), filter holder with Nuclepore filter (Whatman, UK) with a pore size of 0.2 µm, pump (P) and vacuum pump (V).

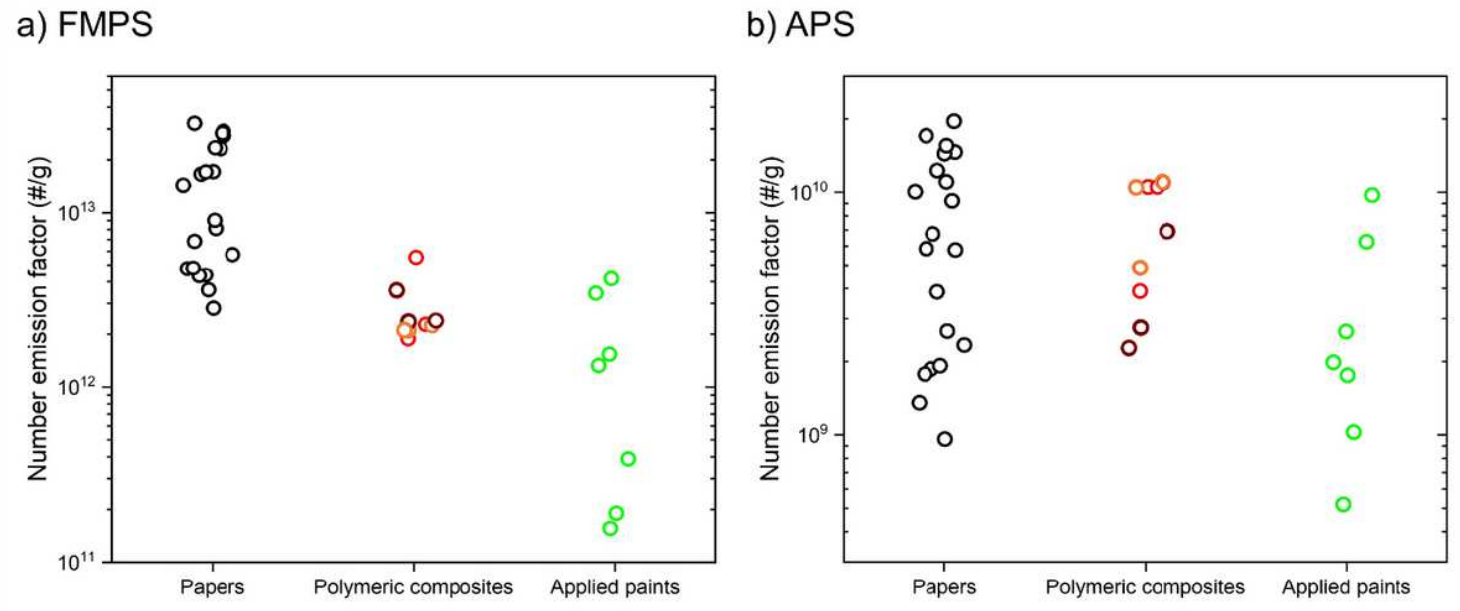

Figure 2

Aerosol number emission factors (#/g) for aerosols from combusted paper with SiO2 or Fe2O3 NMs, polymeric composites (TPU in orange, PA6 in dark red and PLA in red) with CuPhthalocyanine NMs and applied paints on spruce wood panels with SiO2 or Fe2O3 NMs, a) in the FMPS size range of 5.6 nm – 560 nm and b) in the APS size range of 0.542 µm – 20 µm. One circle represents the average of a threefold measurement for the same NEP.

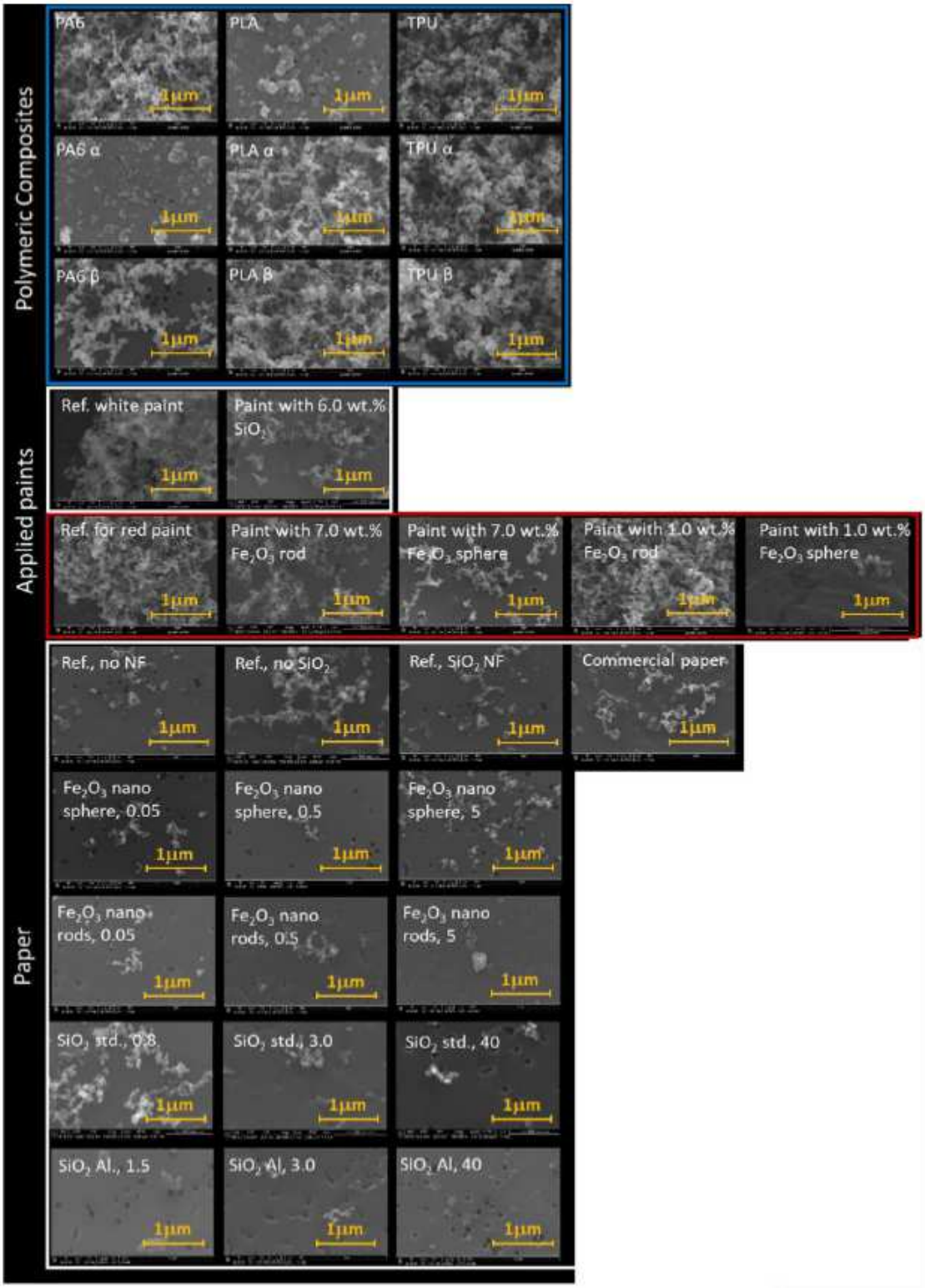

Figure 3

SEM pictures of combustion-generated aerosols from polymeric composites with Cuphthalocyanine nano α and β, applied paints on wood panels with SiO2 and Fe2O3 and paper with SiO2 and Fe2O3.

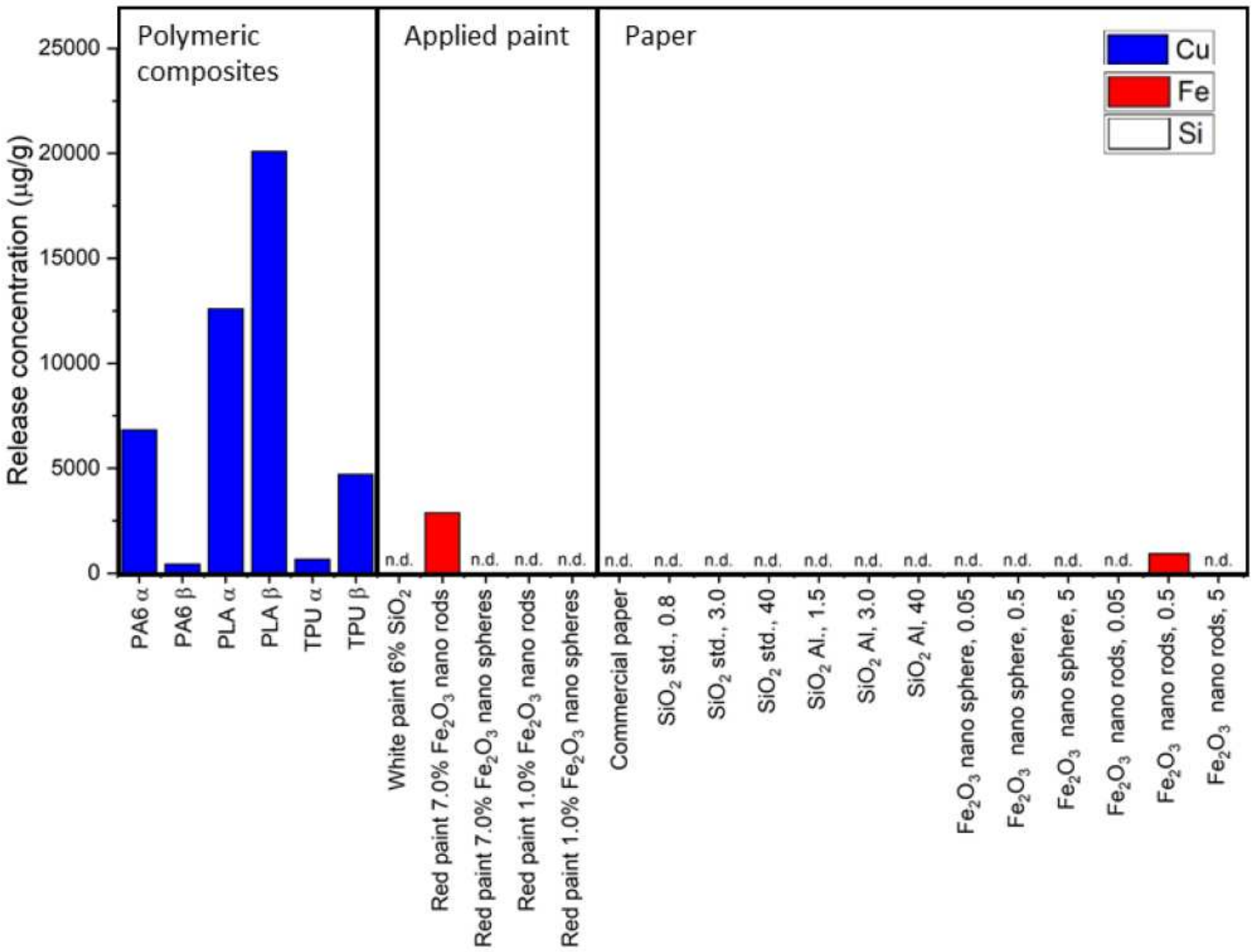

Figure 4

Detected concentrations of Cu, Si and Fe signature elements of the embedded NMs in the aerosols from com-busted polymeric composites with Cuphthalocyanine nano α and Cuphthalocyanine nano β and applied paints on wood panels with SiO2 and Fe2O3 and paper with SiO2 and Fe2O3. N.d. stands for not detected.

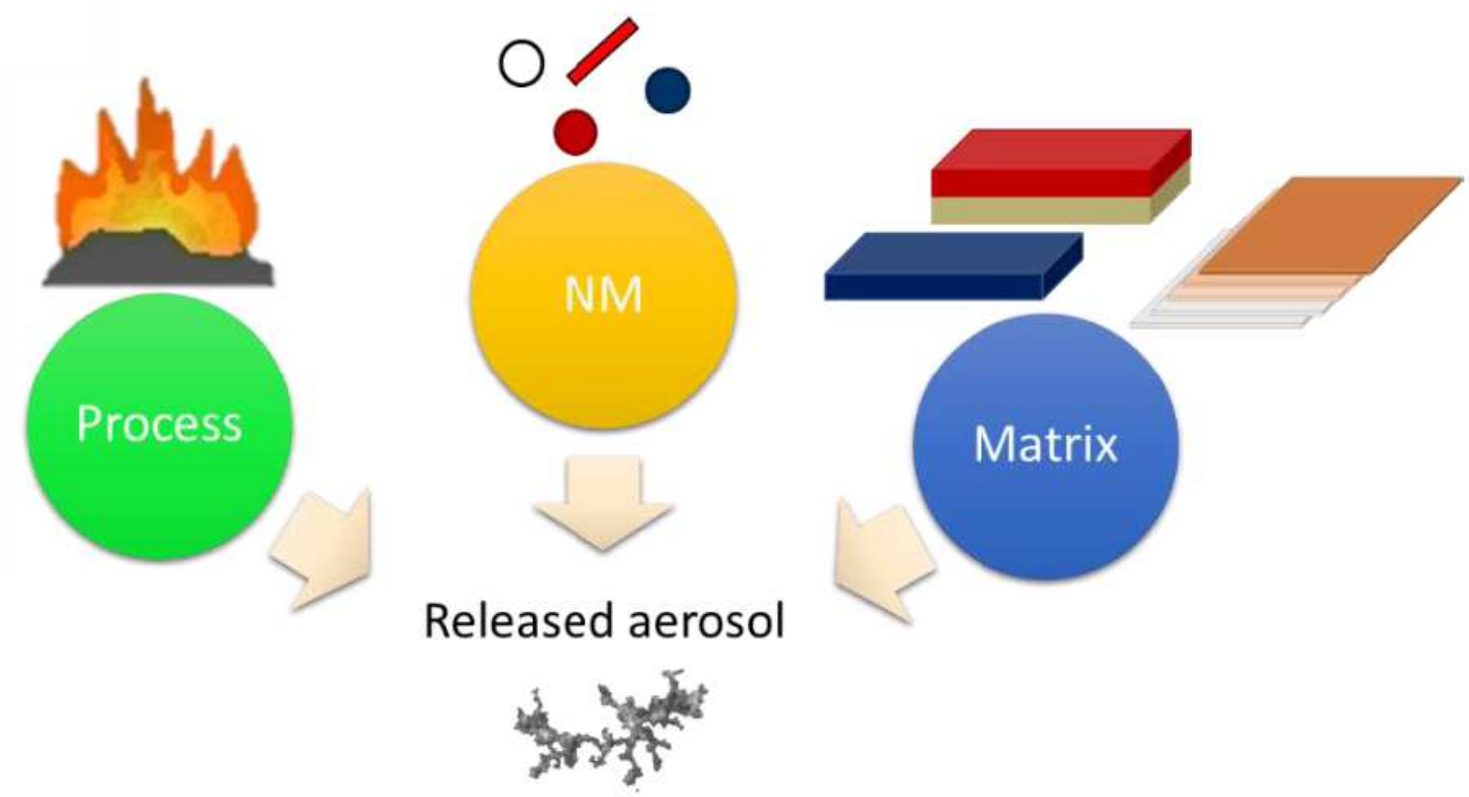

Figure 5

Graphic showing the influence of process, nanomaterial (NM) and matrix on the released aerosol.

Supplementary Files

This is a list of supplementary files associated with this preprint. Click to download.

- 201216Supplementarryinformation.pdf
- Highlights.docx